Carbon 229 (2024) 119456

Contents lists available at ScienceDirect

Carbon

journal homepage: www.elsevier.com/locate/carbon

Research paper

Thermoelectric properties of graphene through BN-ring doping: A theoretical investigation

Laura Caputo *, Viet-Hung Nguyen, Jean-Christophe Charlier

Institute of Condensed Matter and Nanosciences, Université catholique de Louvain (UCLouvain), Chemin des étoiles 8, B-1348, Louvain-la-Neuve, Belgium

ARTICLE INFO

Keywords:
Graphene
Boron and nitrogen doping
Thermoelectric properties
Atomistic simulation

ABSTRACT

Although graphene presents excellent transport properties, its potential for thermoelectric applications is still limited due to its low Seebeck coefficient and high thermal conductivity. Efforts to enhance its thermoelectric properties have involved the usage of carbon-based nanoribbons (Zheng et al., 2012; Hossain et al., 2016) [1,2], strain engineering (Nguyen et al., 2015), and heteroatom co-doping, particularly with nitrogen and/or boron atoms (Wang et al., 2018) [3]. In this work, multiscale simulation approaches combining density functional theory calculations and semi-empirical models are used to investigate the thermoelectric properties of graphene via borazine (B_3N_3)-ring doping. In particular, the bandgap engineering obtained by this doping technique (Caputo et al., 2022) can separate opposite electron and hole contributions and therefore results in a significant enhancement of the Seebeck effect and, accordingly, of the power factor. The results obtained are not only dependent on the concentration of B_3N_3 rings but are also notably influenced by their orientation configuration. Furthermore, the effects of distribution and rotational disorders are also considered, clarifying the thermoelectric properties of realistic systems. Lastly, the thermal lattice conductance is estimated revealing a substantial reduction of up to 40% compared to pristine graphene opening up the possibility of enhancing the thermoelectric efficiency of BNC materials. The present theoretical approach highlights how BN-ring doping can refine the thermoelectric properties of graphene, offering a pathway for enhancing its suitability in practical thermoelectric applications.

1. Introduction

The thermoelectric effect has been known for nearly 200 years, yet new applications continue to emerge. In fact, thermoelectric materials are becoming increasingly important in the search for sustainable and efficient energy solutions, which is essentially due to their ability to turn waste heat into electrical power. This makes thermoelectric materials highly relevant in various applications, including automotive waste heat recovery [4], spacecraft power generation [5], and wearable energy harvesting devices [6]. Initially, the research on bulk materials explored the best thermoelectric properties in alloys of materials such as PbTe, Bi_2Te_3, or $(Bi_{1-x}Sb_x)_2(Se_{1-y}Te_y)_3$ alloy family, and so on [7,8]. However, these bulk materials still exhibit limitations in thermoelectric efficiency and the pioneering works of Hicks and Dresselhaus [9] suggested that nanostructuring materials into low-dimensional systems could improve the performance of thermoelectronic devices. Their research shows that improving the energy-dependent nature of the electronic conductivity (σ) can significantly increase the Seebeck coefficient (S), which is the key parameter of thermoelectric materials. Consequently, low-dimensional systems are expected to offer a higher Seebeck coefficient and accordingly higher power factor ($PF = S^2\sigma$), compared to bulk materials. Note that the thermoelectric efficiency is quantified by the figure of merit $ZT = \sigma S^2 T/\kappa$, where κ represents the thermal conductivity. Therefore, two well-known strategies for improving ZT are either to enhance the power factor or to reduce the thermal conductivity. Enhancing the power factor has also the benefit of increasing the output power of thermoelectric generators [10]. Many nanostructuring methodologies have been studied up to date, including organic materials [11], inorganic materials [12], systems with different dimensionality [13], and other techniques [14–17].

On this basis, graphene has emerged as a promising material, due to its truly 2D crystal structure and excellent transport properties [18,19]. In particular, electrons in graphene behave as massless Dirac fermions near the K-points of its Brillouin zone, leading to the high Fermi velocity ($\sim 10^6$ cm s^{-1}), and accordingly, to high carrier mobilities and high electronic conductivity [19]. However, graphene still presents a limitation when considering thermoelectric applications, basically due to its semi-metallic characteristics. Indeed, opposite contributions of electrons and holes cannot be separated in this gapless material, thus

* Corresponding author.
E-mail address: laura.caputo@uclouvain.be (L. Caputo).

https://doi.org/10.1016/j.carbon.2024.119456
Received 3 April 2024; Received in revised form 3 July 2024; Accepted 18 July 2024
Available online 22 July 2024

resulting in a relatively low Seebeck coefficient [20]. Therefore, notable efforts have been invested in improving the thermoelectric properties of graphene. First and foremost, published studies have focused on the engineering of the Seebeck effect in graphene, particularly, by opening a bandgap in order to separate the electron and hole contributions [20]. Striking examples include graphene nanoribbons [1,2,21–25], graphene antidot superlattices [26–28], and strain engineering [29]. Some of these studies have also proposed nanostructuring techniques to improve the thermoelectric figure of merit ZT (see [20] and references therein).

In the case of graphene 2D monolayer, the general strategy for engineering the bandgap is basically to break its sublattice symmetry. In particular, pristine graphene consists of two symmetrical-triangular sublattices, A and B, which is the origin of its gapless character [19]. Therefore, a bandgap can open in graphene 2D monolayer when the mentioned sublattice symmetry is broken as, for example, obtained by the sublattice selective doping with boron and/or nitrogen atoms [30,31]. Another method to engineer the properties of graphene is to use borazine-like (B_3N_3) doping units [32,33]. By incorporating BN-rings into graphene, boron and nitrogen atoms replace carbon atoms in two different sublattices, thus creating an even larger sublattice asymmetry than that obtained with single dopants. With this doping technique, the electronic properties of graphene are also tunable by controlling the orientation of BN rings [32]. This technique could therefore be an alternative method to engineer the thermoelectric properties of graphene, which will be examined in the current work.

Experimentally, significant efforts have been made to develop new synthetic methods for producing periodic BN-doped covalent carbon networks. Although there have been successful syntheses of BNC structures [34,35], their properties and applications are still not fully explored.

While extensive theoretical investigations of the effects of single dopants [36–38] or *h*-BN domains [3,23,39–41] on graphene thermoelectric properties have been reported, the impact of isolated borazine rings remains, to the best of our knowledge, unexplored. In this context, the current work presents multi-scale calculations of the thermoelectric properties of BN-ring doped graphene monolayers. These calculations allow for comprehensively investigating the dependence on the ring concentration, ring orientation as well as disorder effects. In particular, *ab initio* calculations were first performed for systems obtained when BN-rings are periodically inserted into graphene. Non-periodic doped systems were then computed using a semi-empirical tight-binding model to depict more realistic scenarios and highlight the impact of the disorder on these properties. At last, to estimate the thermoelectric efficiency of the considered BNC materials, the lattice thermal conductivity (using atomistic force constant models) and accordingly the thermoelectric figure of merit ZT were also computed.

2. Methologies

Transport calculations have been performed on a device, as schematized in Fig. 1. In particular, the device channel is a BNC 2D monolayer where charge carriers and heat transmit between left (hot) and right (cold) contacts (reservoirs). This implies that the transport channel is assumed to be very large in both in-plane directions, i.e., exceeding hundreds of nm so as to avoid the finite-size confinement as well as edge effects. Therefore, calculations can be performed using the periodic boundary condition in the direction that is perpendicular to the transport one.

As discussed, periodically doped BNC networks can be achieved using bottom-up techniques [34]. Therefore, our study first focuses on such cases and first-principles calculations are conducted to compute thermoelectric properties of periodically doped systems. These calculations are performed using the combination of Density Functional Theory (DFT) framework and Green's function (GF) approach in the ballistic approximation, as implemented in OpenMX code [42–44]. The generalized-gradient approximation of Perdew Burke and Ernzherof (PBE) [45] has been exploited for the exchange–correlation density functional and the electron-ion interaction is described with norm-conserving pseudopotentials as proposed by Morrison et al. [46]. *Ab initio* calculations have been performed with the usage of a numerical pseudo-atomic orbitals as basis set, decomposed in two *s*-orbitals, two *p*-orbitals and one *d*-orbital for each of the atom types. The energy cutoff for real-space mesh has been chosen to be 300Ry while a k-point grid of $33 \times 33 \times 1$ for the graphene unit cell has been employed. Moreover, an interlayer vacuum distance of 20 Å has been employed to avoid spurious interaction along the non-periodic z direction. To investigate different BN doping scenarios, a 5×5 supercell was built from the orthorhombic unit cell of graphene and consequently doped with BN rings to create models with varying concentrations. Each atomistic model underwent full relaxation of in-plane cell parameters and atomic positions. Note that as this work investigates 2D graphene sheets, the dependence on the transport direction is not very significant at low energies (i.e., near the gap region as illustrated in Fig. S1). Moreover, our study focuses on the BN-ring doping effects and therefore the transport along the armchair direction (as illustrated in Fig. 1) was computed and discussed. In addition, when incorporating a BN-ring into graphene, boron and nitrogen atoms replace C atoms in two different (A and B) sublattices of graphene, respectively. However, this doping configuration is reversed when the ring is rotated by 60°. Therefore, two distinct scenarios arise: parallel orientation (i.e., all rings are in the same orientation) and anti-parallel orientation (i.e., there is a mixture of opposite-oriented rings) cases. Both these cases were investigated by our DFT calculations and the concentration of anti-parallel rings was also taken into account.

The thermoelectric quantities were computed in terms of the electronic transmission (T_e) using the Landauer-Büttiker formalism. In particular, this involves computing the auxiliary function L_n as

$$L_n(\mu,T) = \int T_e(E)(E-\mu)^n \left[-\frac{\partial f_e(E,\mu,T)}{\partial E}\right] dE \tag{1}$$

where μ is the electron chemical potential and $f_e(E,\mu,T)$ is the Fermi-Dirac distribution function. The electronic conductance G, the Seebeck coefficient S and the electronic thermal conductance K_e were calculated as

$$G(\mu,T) = \frac{2e^2}{h} L_0(\mu,T) \tag{2}$$

$$S(\mu,T) = \frac{1}{eT}\frac{L_1(\mu,T)}{L_0(\mu,T)} \tag{3}$$

$$K_e(\mu,T) = \frac{1}{T}\left[L_2(\mu,T) - \frac{L_1(\mu,T)^2}{L_0(\mu,T)}\right] \tag{4}$$

The thermoelectric properties of aperiodic (i.e., disordered) systems are also investigated. In this case, as the periodic boundary conditions can no longer be applied to a relatively small unit cell, the number of atoms to compute is huge (i.e., a few hundred thousand), making DFT calculations unfeasible. Therefore, a first principles-enriched tight-binding (TB) Hamiltonian [32] was used (see section 4 of Supplementary Material). In addition, the recursive Green's function techniques [47] were also applied to solve the corresponding heavy calculations of these disordered systems.

At last, to compute the lattice thermal conductance, the dynamical properties were modeled using the fourth nearest-neighbor force constant (4NN FC) model. In particular, the FC parameters in Ref. [48] for C–C bonds and in Ref. [49] for B-N bonds were used. For the coupling of C atoms with B and N atoms, the average values of the FC parameters of graphene and *h*-BN were considered [23,40]. The recursive Green's function method [47] was again used to solve the mentioned FC model and to compute the phonon transmission $T_p(\omega)$. The lattice thermal conductivity was then calculated as

$$K_l = \int_0^\infty \frac{d\omega}{2\pi} \hbar\omega T_p(\omega) \frac{\partial n(\omega,T)}{\partial T} \tag{5}$$

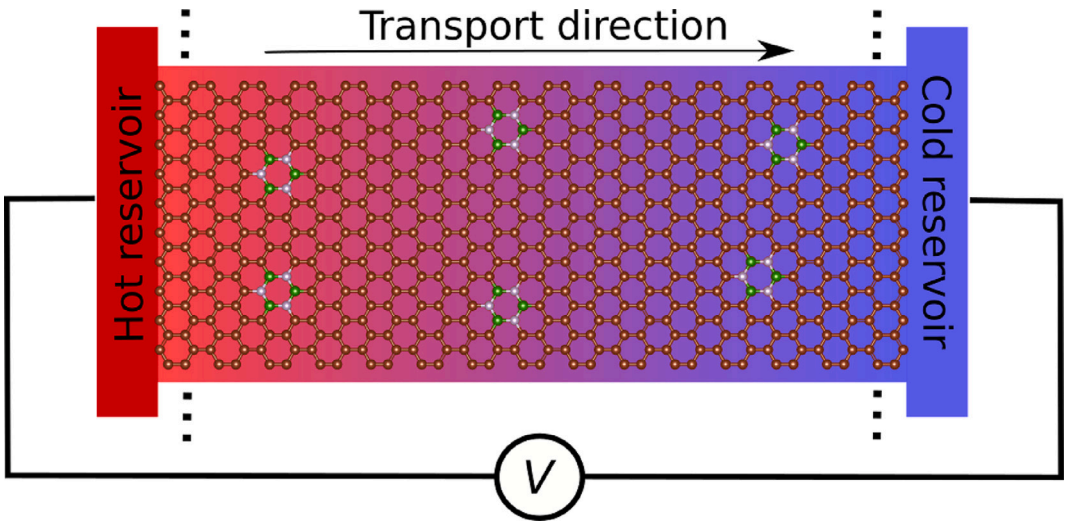

Fig. 1. Schematic model of a typical thermoelectric device built with a BNC material. The transport direction is defined from the hot (red) to the cold (blue) reservoir. The central region is formed by a periodically boron and nitrogen co-doped graphene layer. The model is periodic in the in-plane direction perpendicular to the transport, denoted with dashed black lines. Brown, green and gray spheres represent carbon, boron and nitrogen atoms, respectively. (For interpretation of the references to color in this figure legend, the reader is referred to the web version of this article.)

where $n(\omega, T)$ is the Bose–Einstein distribution function. The thermoelectric figure of merit was evaluated using the standard formula:

$$ZT = \frac{S^2 G}{K_e + K_l} T \tag{6}$$

Here, the total thermal conductance is a sum of electron (K_e) and lattice (K_l) thermal parts.

In addition, note that the electron–phonon interactions have been shown to be notably weak in monolayer graphene [50], as indeed, high carrier mobilities $\gtrsim 10^5$ cm^2 V s^{-1} can be obtained either in suspended graphene or in graphene/*h*-BN [51,52]. Consequently, the ballistic electron transport model can compute well micrometer scale devices [53]. Moreover, the ballistic transport calculations have been also demonstrated to be a good approximation for phonons in monolayer graphene at room temperature [54]. Interestingly, similar to pristine graphene, boron-nitride embedded graphene has also exhibited high carrier mobilities [55,56]. Therefore, ballistic transport calculations is assumed as a good approximation for the BNC devices considered herewith. Note that the ballistic approximation in the current work implies that many-body interactions are neglected but scatterings with BN rings are still present in our calculations. Finally, calculations were performed at room temperature throughout the work.

3. Discussion

3.1. Improved thermoelectric effects

Firstly, the effect of BN concentration in monolayer graphene is considered by DFT calculations. In particular, six distinct percentage concentrations (Model 1 – 6%, Model 2 – 12%, Model 3 – 18%, Model 4 – 24% and Model 5 – 36%) with an increase of the number of borazine rings (two, three, four and six rings, respectively, see Fig. 2a) in the graphene supercell were examined. To focus on the effects when varying the ring concentration, all BN-rings are in the same orientation, i.e., parallel configurations. The computed electronic conductances (G), Seebeck coefficients (S), Power Factors ($PF = S^2G$) and electronic thermal conductances (K_e) are presented in Fig. 2. As mentioned, pristine graphene exhibits ambipolar characteristics (i.e., semi-metallic behavior) and therefore both electrons and holes can present significant contributions to its thermoelectric properties when the charge-carrier concentration is low. Therefore, the opposite contributions of these two carrier types lead to a small Seebeck effect. In particular, a Seebeck coefficient smaller than 100μV K^{-1} at room temperature has been experimentally reported [57]. Indeed, this aligns closely with our calculations, as presented in Fig. 2d.

When BN-ring doping is introduced, the Seebeck coefficient and the PF significantly increase with increasing the doping concentration (see Figs. 2c and 2d). In particular, their obtained values can be an order of magnitude higher than that of pristine graphene (i.e., see the results of models 4 and 5). In addition, a nearly linear increase of these quantities with the BN concentration is found. Additionally, it is worth noting that besides the applications as in devices with large Seebeck effects, a large PF is also beneficial for thermoelectric generators as it corresponds to a large output power density. However, these results are obtained at the cost of the reduction of electronic conductance, as a bandgap opens and the doping induces scatterings in graphene.

For more details, note that the sublattice symmetry of graphene is most strongly broken for a given concentration of BN rings when they present the same orientation, i.e. parallel case. This is because all nitrogen (boron, respectively) atoms selectively replace C atoms in the single A (B, respectively) sublattice of graphene. This sublattice symmetry breaking leads to a bandgap opening in graphene [32] and consequently, a transport gap as illustrated by the computed conductance in Fig. 2b. Even though the conductance is reduced, the presence of these gaps separates electron and hole contributions, which is essentially the reason for the increase of the Seebeck coefficients with increasing the doping concentration, seen in Fig. 2d. Even though these two quantities present opposite trends with the doping effects, the PF (=S^{2}G) still increases (Fig. 2c), similar to the property of S. Note that at room temperature, the width of thermal broadening is effectively about 0.2 eV. Therefore, a band gap ~0.2 eV could present the best compromise for a large Seebeck coefficient while the conductance is still high at room temperature. In particular, the best compromise could be obtained with the BN concentration of ~12% (Model 2) as presented in Fig. 2.

The electronic contribution to the thermal conductance K_e is presented in Fig. 2e. Actually, the effects of BN-ring doping on this quantity are similar to those obtained for the electronic conductance in Fig. 2b.

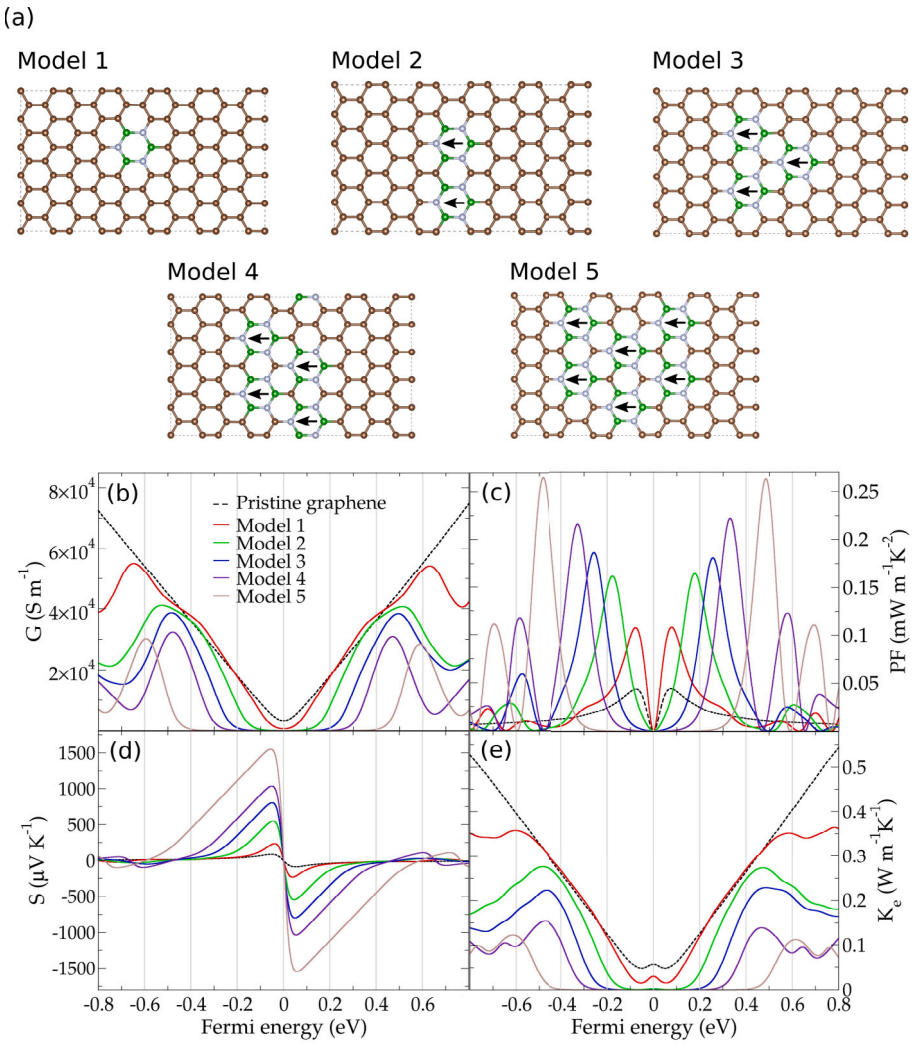

Fig. 2. (a) Atomistic models of graphene doped with various BN-ring concentrations in the parallel orientation and their corresponding (b) electronic conductance (G), (c) power factor (PF), (d) Seebeck coefficient (S), (e) electronic thermal conductance (K_e) as a function of the Fermi level. Pristine graphene (0% BN-concentration) is reported with a black dashed line as a reference.

Interestingly, while a large electronic conductance is beneficial for achieving large value of PF and, accordingly, of ZT, reducing the thermal conductance is another strategy to enhance the thermoelectric efficiency. Therefore, the increase of PF and the reduction of electronic thermal conductance can contribute to the increase of ZT, which will be detailed below in Section 3.3.

As suggested by the study in Ref. [32], another important doping parameter that can be used to tune the thermoelectric properties of the BNC systems above is the orientation of BN-rings. In particular, when certain BN rings in the supercell of these systems (see Fig. 2a) are rotated by 60°, a mixture of BN rings in two opposite orientations are obtained as illustrated in Figs. 3a and 4a. We refer to these cases as anti-parallel orientation structures herewith. In the cases studied in Figs. 3 and 4 (other systems also presented in section 3 of Supplementary Material), the anti-parallel configurations are characterized by the percentage of rotated rings with respect to the total number of rings within the supercell. Indeed, when the number of rotated (or anti-parallel) rings increases, the transport properties and, accordingly, the thermoelectric properties substantially change. In particular, the transport gap is narrowed, consequently the electronic conductance (Figs. 3a and 4a) and electronic thermal conductance (Figs. 3e and 4e) increase with increasing the percentage of anti-parallel rings. However, the Seebeck coefficient (Figs. 3d and 4d) and PF (Figs. 3c and 4c) are generally reduced. These results can be essentially explained by the dependence of graphene's sublattice asymmetry induced by this doping technique on the rotation of BN rings [32]. In particular, when certain rings are in the anti-parallel orientation, there are both boron and nitrogen atoms replacing C atoms in each of the two sublattices of graphene. This diminishes its sublattice asymmetry, compared to the fully parallel case, thus reducing the obtained bandgap and explaining the presented results. It is suggested that the discussed orientation dependence can be exploited to obtain the best compromise between high electronic conductance and low thermal conductance. In particular, a large doping concentration can result in a strong reduction of both these quantities but rotating a certain number of BN rings can increase the electronic conductance again.

At last, the dependence on the distribution of BN-rings within the DFT supercell (see an example, Model 2, presented in section 2 of Supplementary Material) was also examined. However, the transport properties around the band gap, and consequently, the thermoelectric effects are weakly affected by the change in the position of BN rings. This could be considered a beneficial point of this doping technique as it can make experiments more feasible.

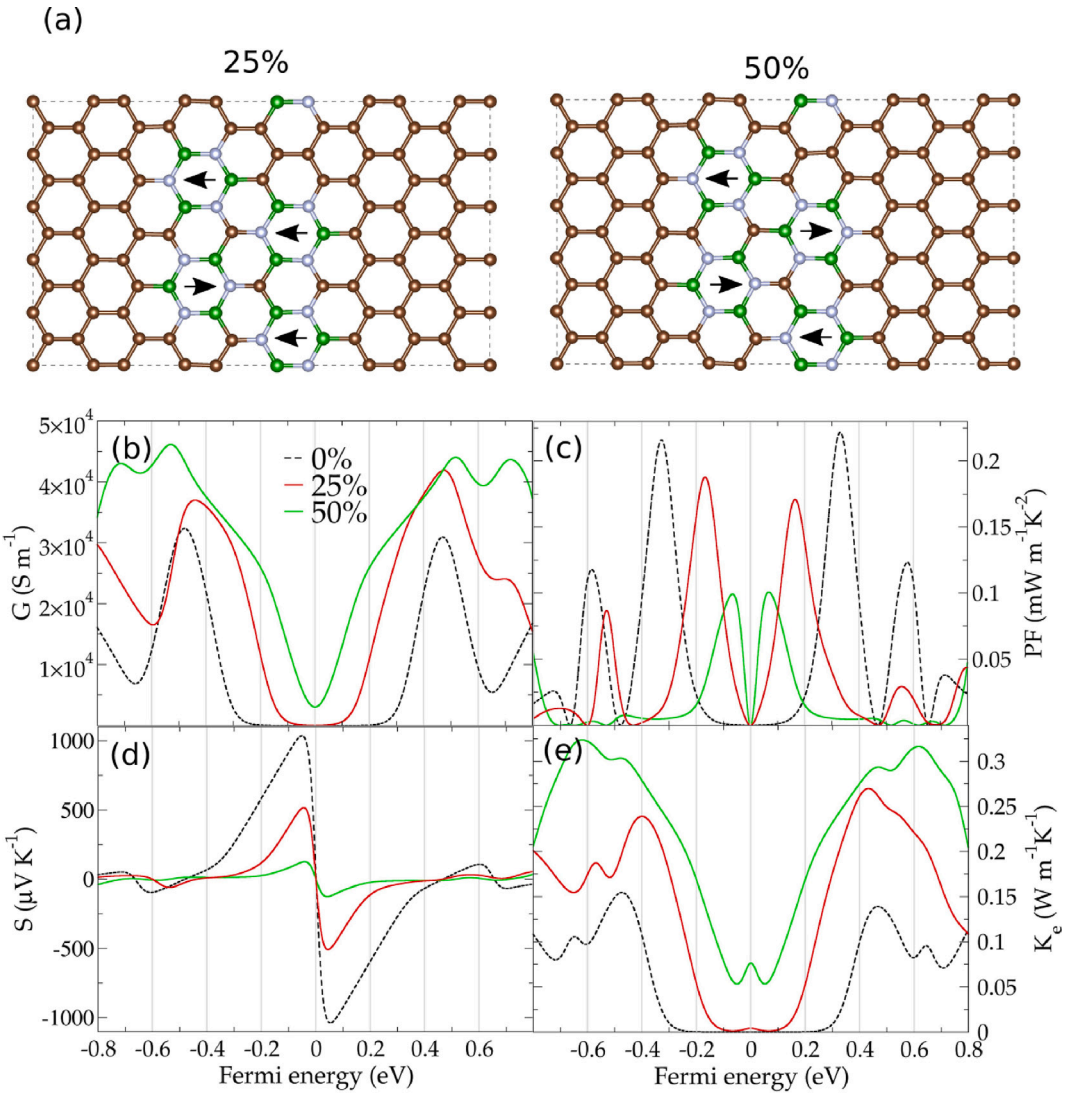

Fig. 3. (a) Atomic structures of Model 4 with 25% and 50% anti-parallel rings and their corresponding (b) electronic conductance, (c) power factor, (d) Seebeck coefficient and (e) electronic thermal conductance. The same Model 4 with all parallel orientation (0% anti-parallel rings) of the BN-rings pointing in the same direction is reported as a black dashed line.

3.2. Disorder effects

Even though periodically doped systems can be expectedly obtained by bottom-up techniques, doping disorders are, in principle, a practical issue [58,59] and must still be consider. The current work focuses on two important disorders related to the distribution and orientation of BN rings. To compute the effects of these disorders, devices consisting of a large BN-ring doped graphene (particularly, ~154 nm × 37 nm) domain, connected to two pristine graphene leads, are considered. Such large BN-doped domain is periodic in the perpendicular direction and was formed by repeating periodically 4 × 3 orthorhombic supercell containing a single BN ring. Disorders were then obtained by changing the position (distribution disorder) or by rotating (rotational disorder) certain BN rings in the doped region. In the first case, certain BN-rings are randomly displaced to neighboring positions relative to their locations in the ordered (i.e., perfectly periodic) system, while in the second case, a certain number of rings are randomly rotated. Similarly, the details of these disorder models can be found in Ref. [32]. Consideration of these small displacements is actually based on the assumption that, as mentioned, bottom-up techniques are expected to control the periodicity of BN rings, and therefore, only weak disorders are likely to appear. To compute these large disordered systems, DFT calculations are unfeasible and therefore tight-binding models were employed. The effects of both disorder types were computed and presented in Fig. 5, where the results for the perfectly periodic system (dashed black line) were also added for comparison.

Consistently with our previous study [32], the distribution disorder presents negligible effects on the bandgap and accordingly, on the transport gap (see the top panel of Fig. 5a). However, these gaps are significantly reduced with increasing the rotational disorder (see the top panel of Fig. 5b), similar to the DFT results in the anti-parallel cases. Even though weakly affecting the transport gap, the distribution disorder still presents significant effects on electronic conductance and electronic thermal conductance. Consequently, the PF can be substantially affected (i.e., reduced), although the Seebeck coefficient is not. On the other hand, the rotational disorder clearly exhibits different effects. First, the bandgap and transport gap are reduced, leading to the enhancement of the electronic conductance and electronic thermal conductance at low energies. However, the scatterings induced by such disorder still reduce these two conductances at large energies. Finally, both the Seebeck coefficient and the PF are affected (i.e., reduced) by increasing the rotational disorder. Our presented results suggest that a good control of the doping configuration, with only a small amount of disorder (e.g, a few to ten percent), could be beneficial for practical applications.

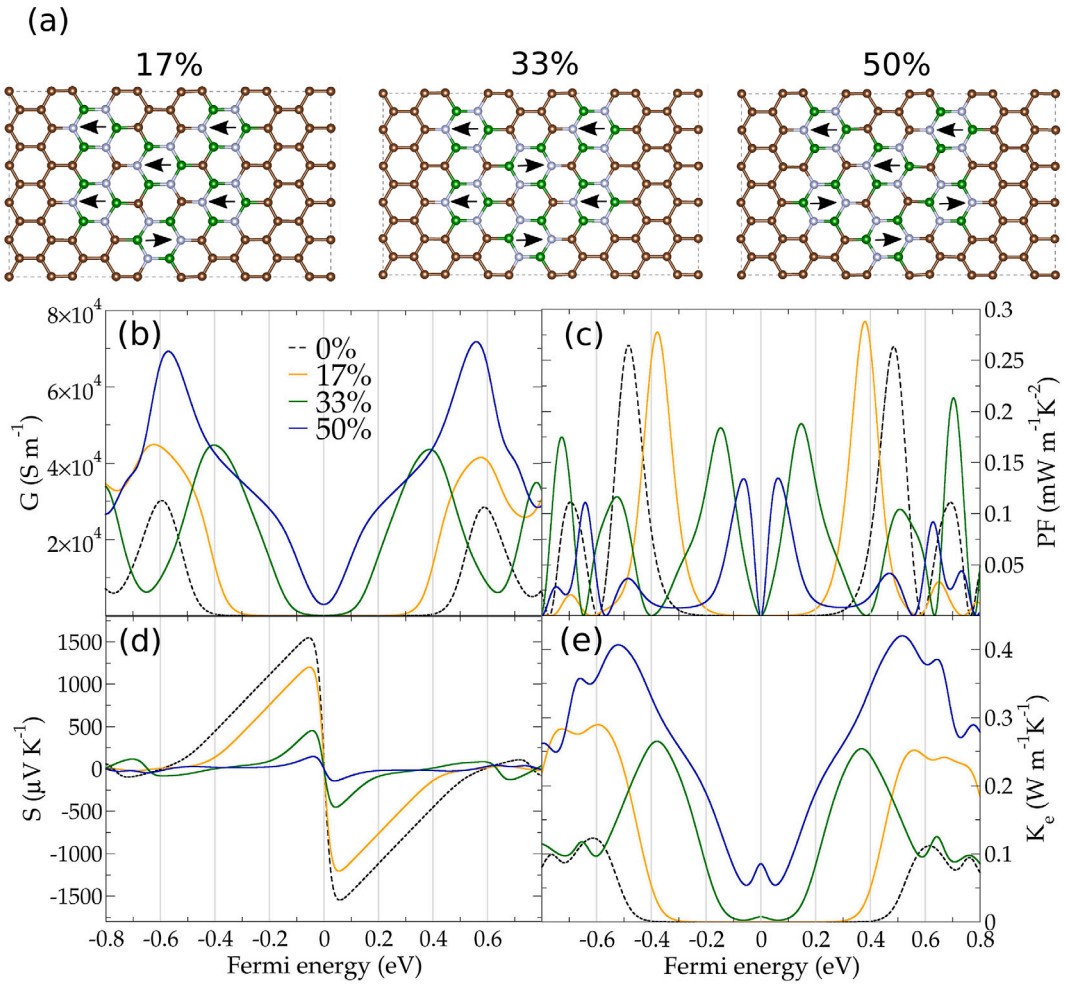

Fig. 4. (a) Atomic structures of Model 5 with 17%, 33% and 50% anti-parallel rings and their corresponding (b) electronic conductance, (c) power factor, (d) Seebeck coefficient, (e) electronic thermal conductance. The same Model 5 with all parallel orientation (0% anti-parallel rings) of the BN-rings pointing in the same direction is reported as a black dashed line.

3.3. Thermoelectric efficiency

As earlier mentioned, pristine graphene exhibits an exceptionally high thermal conductivity [60] and accordingly, its thermoelectric figure of merit is extremely low, i.e., below 0.01 [20]. Therefore, reducing the lattice thermal conductance is also necessary for improving the thermoelectric efficiency of this material.

With the presented enhancement of thermoelectric properties, the thermoelectric efficiency of the considered BN-ring doped graphene is now estimated. For this estimation, the lattice thermal conductance was computed by the force constant model described in Section 2. In Table 1, the lattice thermal conductance K_l is presented for different doping configurations considered in Section 3.1. Obviously, this conductance is substantially reduced by increasing the doping concentration. Indeed, a large reduction of about 40% is obtained for Model 5 with all parallel rings. However, the rotation of BN rings presents negligible effects on the lattice thermal conductance. These results could be explained by the fact that the sublattice asymmetry strongly affects the electronic transport but not the thermal one.

Combining the electronic transport quantities in Section 3.1 and the lattice thermal conductance here, the figure of merit ZT is estimated. In Fig. 6, ZT values for the five doping Models with all parallel rings, as depicted in Fig. 2, are presented. The results obtained for different anti-parallel configurations of these models are also discussed in Section 5 of Supplementary Material. As the PF increases and K_l is reduced, the ZT increases with increasing the doping concentration. The largest ZT, ~0.1, is achieved here for the Model 5. Even though not too large, these results are still a significant improvement, i.e., more than ten times larger than the value in pristine graphene. Actually, since the phonon properties of *h*-BN are not very different from those of graphene, the presented doping technique cannot reduce more strongly the lattice thermal conductance. However, a combination of this technique with other nanostructuring ones (for example, cross-plane and other heterostructures [15,61–64]) could be a good suggestion for more efficient

Table 1
Lattice thermal conductance (in W K^{-1}m^{-1}) calculated with the 4NN FC model for pristine graphene and BN-ring doped systems with Models 1, 2, 3, 4 and 5 (see Fig. 2). For each BN-ring doped system, possible anti-parallel (0%, 17%, 33% or 50%) configurations are considered.

K_l (W m^{-1} K^{-1})	0%	17%	33%	50%
Graphene	1.31			
Model 1	1.08	–	–	–
Model 2	0.96	–	–	0.98
Model 3	0.88	–	0.88	–
Model 4	0.86	–	0.86	0.86
Model 5	0.80	0.80	0.79	0.81

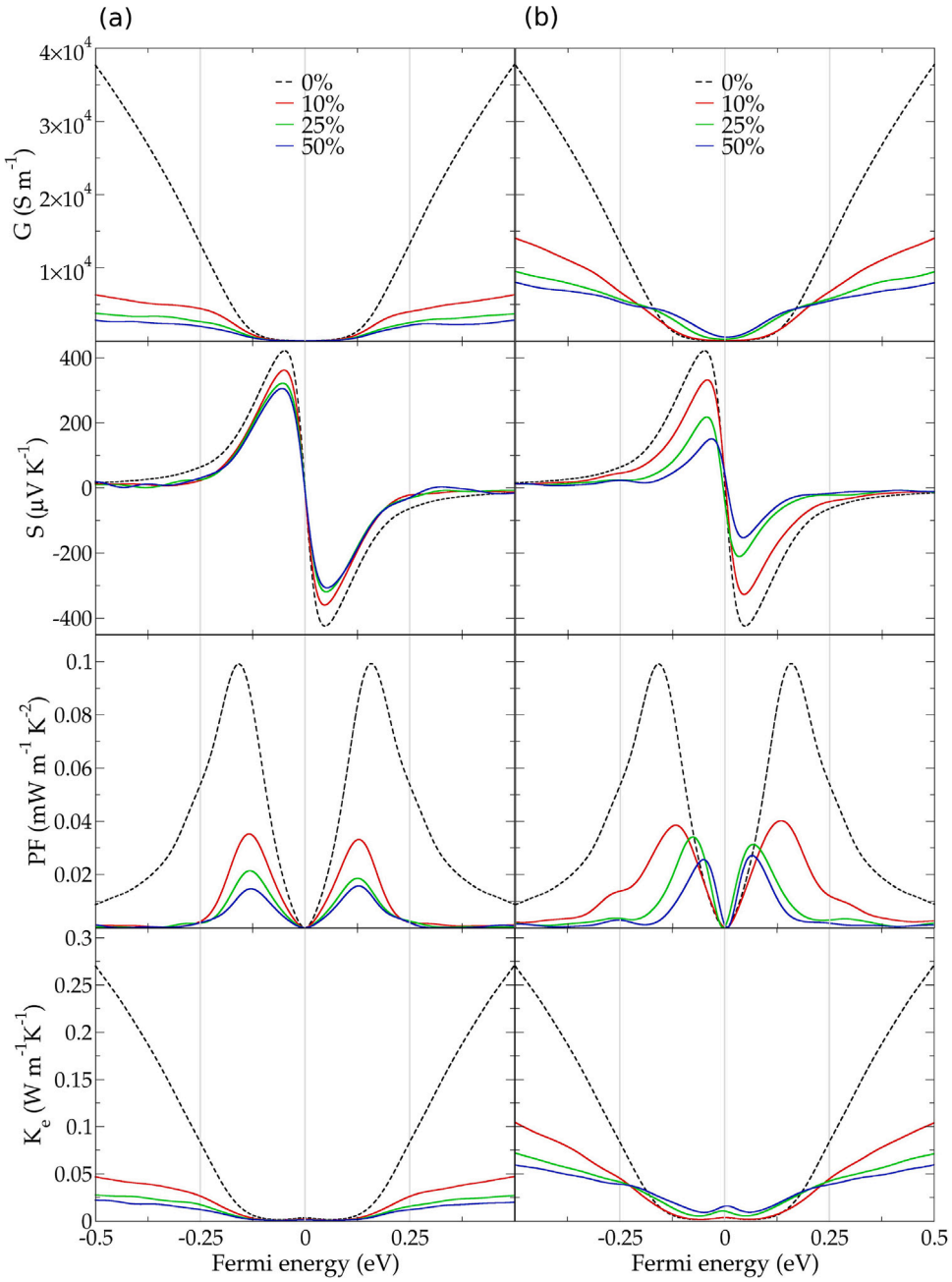

Fig. 5. Electronic conductance, Seebeck coefficient, Power Factor and electronic thermal conductance for (a) distribution disorder and (b) rotational disorder computed within a tight-binding approach. Different disorder strengths, 10%, 25% and 50% are investigated while the perfectly periodic case (0% disorder strength) is also reported in dashed black line. The BN-ring concentration is 12.5% in all cases.

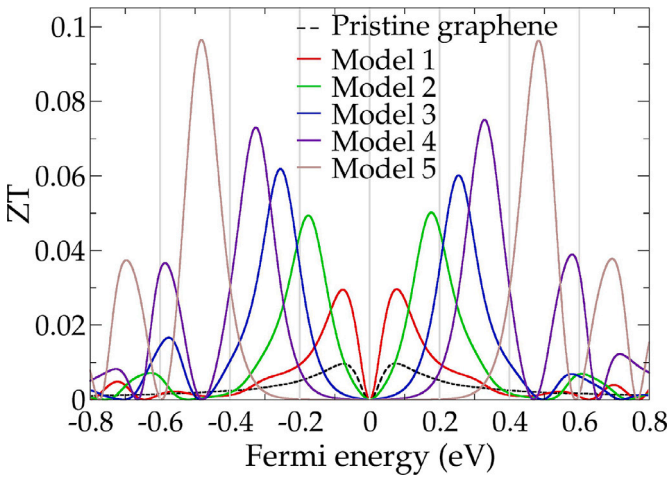

Fig. 6. Thermoelectric figure of merit ZT computed for BN-ring doped graphene systems with all parallel rings as considered in Fig. 2. ZT of pristine graphene (0% BN-concentration) is reported in dashed black line.

thermoelectric devices. In fact, the cross-plane heterostructures proposed in Ref. [61,62] can exhibit a very strong reduction of thermal conductance but engineering the bandgap is still needed.

4. Conclusions

Using multiscale atomistic calculations, this work explores how the thermoelectric properties of graphene can be improved by BN ring doping. Indeed, the presence of BN rings in the graphene lattice induces the breaking of its sublattice symmetry, thus leading to the opening of bandgap and, accordingly, of transport gap in the considered devices. Thereby, opposite electron and hole contributions can be efficiently separated, leading to the significant enhancement of thermoelectronic properties of graphene. In particular, an increase by one order of magnitude in Seebeck coefficient, Power Factor, and ZT can be obtained. The study also shows that the results are strongly dependent on the ring orientation but weakly sensitive to the ring distribution. In particular, the transport gap is largest if all rings are parallel and is reduced by controlling the rotation of the rings. The effects of disorder were also estimated, suggesting that a good control of doping configurations (i.e., about $\lesssim 10\%$ distribution and rotational disorders) can be promising for practical applications. Overall, the enhanced thermoelectric effects can largely extend the practical applications of graphene. Moreover, even though it cannot reduce very strongly the thermal conductance (only about 40% reduction is reported here), the considered doping technique can be combined with other nanostructuring techniques for designing more efficient thermoelectronic devices.

CRediT authorship contribution statement

Laura Caputo: Writing – review & editing, Writing – original draft, Visualization, Validation, Investigation, Formal analysis, Data curation. **Viet-Hung Nguyen:** Writing – review & editing, Writing – original draft, Visualization, Validation, Supervision, Methodology, Investigation, Formal analysis, Data curation, Conceptualization. **Jean-Christophe Charlier:** Writing – review & editing, Validation, Supervision, Resources, Project administration, Methodology, Investigation, Funding acquisition, Formal analysis, Data curation, Conceptualization.

Declaration of competing interest

The authors declare that they have no known competing financial interests or personal relationships that could have appeared to influence the work reported in this paper.

Acknowledgments

The authors acknowledge fundings from the European Union's Horizon 2020 Research and Innovation programme under the Marie Sklodowska-Curie entitled "STiBNite" (N° 956923), from the Flag-Era JTC project "MINERVA" (N° R.8006.21), from the Pathfinder Project "FLATS" (N° 101099139), from the Fédération Wallonie-Bruxelles through the ARC project "DREAMS" (N° 21/26-116), from the EOS project "CONNECT" (N° 40007563) and from the Belgium F.R.S.-FNRS through the research project (N° T.029.22F). Computational resources have been provided by the CISM supercomputing facilities of UCLouvain and the CÉCI consortium funded by F.R.S.-FNRS of Belgium (N° 2.5020.11).

Appendix A. Supplementary data

Supplementary material related to this article can be found online at https://doi.org/10.1016/j.carbon.2024.119456.

References

[1] H. Zheng, H. Liu, X. Tan, H. Lv, L. Pan, J. Shi, X. Tang, Enhanced thermoelectric performance of graphene nanoribbons, Appl. Phys. Lett. 100 (9) (2012) 093104.
[2] M.S. Hossain, D.H. Huynh, P.D. Nguyen, L. Jiang, T.C. Nguyen, F. Al-Dirini, F.M. Hossain, E. Skafidas, Enhanced thermoelectric performance of graphene nanoribbon-based devices, J. Appl. Phys. 119 (12) (2016) 125106.
[3] J. Wang, X. Mu, X. Wang, N. Wang, F. Ma, W. Liang, M. Sun, The thermal and thermoelectric properties of in-plane C-BN hybrid structures and graphene/h-BN van der waals heterostructures, Mater. Today Phys. 5 (2018) 29–57.
[4] B. Orr, A. Akbarzadeh, M. Mochizuki, R. Singh, A review of car waste heat recovery systems utilising thermoelectric generators and heat pipes, Appl. Therm. Eng. 101 (2016) 490–495.
[5] F. Ritz, C. Peterson, Multi-mission radioisotope thermoelectric generator (MMRTG) program overview, IEEE Aerosp. Conf. Proc. 5 (2004) 2957.
[6] A. Nozariasbmarz, H. Collins, K. Dsouza, M.H. Polash, M. Hosseini, M. Hyland, J. Liu, A. Malhotra, F.M. Ortiz, F. Mohaddes, V.P. Ramesh, Y. Sargolzaeiaval, N. Snouwaert, M.C. Özturk, D. Vashaee, Review of wearable thermoelectric energy harvesting: From body temperature to electronic systems, Appl. Energy 258 (2020) 114069.
[7] H. Goldsmid, A. Sheard, D. Wright, The performance of bismuth telluride thermojunctions, Br. J. Appl. Phys. 9 (9) (1958) 365.
[8] G.J. Snyder, E.S. Toberer, Complex thermoelectric materials, Nat. Mater. 7 (2) (2008) 105–114.
[9] L.D. Hicks, M.S. Dresselhaus, Effect of quantum-well structures on the thermoelectric figure of merit, Phys. Rev. B 47 (19) (1993) 12727.
[10] W. Liu, H.S. Kim, Q. Jie, Z. Ren, Importance of high power factor in thermoelectric materials for power generation application: A perspective, Scr. Mater. 111 (2016) 3–9.
[11] Y.-J. Zeng, D. Wu, X.-H. Cao, W.-X. Zhou, L.-M. Tang, K.-Q. Chen, Nanoscale organic thermoelectric materials: measurement, theoretical models, and optimization strategies, Adv. Funct. Mater. 30 (8) (2020) 1903873.
[12] G. Schierning, Silicon nanostructures for thermoelectric devices: A review of the current state of the art, Phys. Status Solidi (A) 211 (6) (2014) 1235–1249.
[13] T.G. Novak, K. Kim, S. Jeon, 2D and 3D nanostructuring strategies for thermoelectric materials, Nanoscale 11 (42) (2019) 19684–19699.
[14] C.-W. Wu, X. Ren, G. Xie, W.-X. Zhou, G. Zhang, K.-Q. Chen, Enhanced high-temperature thermoelectric performance by strain engineering in biOCl, Phys. Rev. Appl. 18 (1) (2022) 014053.
[15] H. Pan, L.-M. Tang, K.-Q. Chen, Quantum mechanical modeling of magnon-phonon scattering heat transport across three-dimensional ferromagnetic/nonmagnetic interfaces, Phys. Rev. B 105 (6) (2022) 064401.
[16] Z.-K. Ding, Y.-J. Zeng, W. Liu, L.-M. Tang, K.-Q. Chen, Topological phonons and thermoelectric conversion in crystalline materials, Adv. Funct. Mater. (2024) 2401684.
[17] Z.-K. Ding, Y.-J. Zeng, H. Pan, N. Luo, J. Zeng, L.-M. Tang, K.-Q. Chen, Edge states of topological acoustic phonons in graphene zigzag nanoribbons, Phys. Rev. B 106 (12) (2022) L121401.
[18] A.K. Geim, K.S. Novoselov, The rise of graphene, Nature Mater. 6 (3) (2007) 183–191.
[19] A.H. Castro Neto, F. Guinea, N.M.R. Peres, K.S. Novoselov, A.K. Geim, The electronic properties of graphene, Rev. Modern Phys. 81 (2009) 109–162.
[20] P. Dollfus, V.H. Nguyen, J. Saint-Martin, Thermoelectric effects in graphene nanostructures, J. Phys.: Condens. Matter. 27 (13) (2015) 133204.
[21] F. Mazzamuto, V.H. Nguyen, Y. Apertet, C. Caër, C. Chassat, J. Saint-Martin, P. Dollfus, Enhanced thermoelectric properties in graphene nanoribbons by resonant tunneling of electrons, Phys. Rev. B 83 (23) (2011) 235426.

[22] H. Sevinçli, C. Sevik, T. Çağın, G. Cuniberti, A bottom-up route to enhance thermoelectric figures of merit in graphene nanoribbons, Sci. Rep. 3 (1) (2013) 1228.
[23] V.-T. Tran, J. Saint-Martin, P. Dollfus, High thermoelectric performance in graphene nanoribbons by graphene/BN interface engineering, Nanotechnology 26 (49) (2015) 495202.
[24] V.-T. Tran, J. Saint-Martin, P. Dollfus, S. Volz, Optimizing the thermoelectric performance of graphene nano-ribbons without degrading the electronic properties, Sci. Rep. 7 (1) (2017) 2313.
[25] S. Deng, L. Li, P. Rees, Bilayer graphene nanoribbons junction with aligned holes exhibiting high ZT values, Carbon 155 (2019) 438–444.
[26] H. Karamitaheri, M. Pourfath, R. Faez, H. Kosina, Geometrical effects on the thermoelectric properties of ballistic graphene antidot lattices, J. Appl. Phys. 110 (5) (2011) 054506.
[27] T. Gunst, T. Markussen, A.-P. Jauho, M. Brandbyge, Thermoelectric properties of finite graphene antidot lattices, Phys. Rev. B 84 (2011) 155449.
[28] J. Oh, H. Yoo, J. Choi, J.Y. Kim, D.S. Lee, M.J. Kim, J.-C. Lee, W.N. Kim, J.C. Grossman, J.H. Park, S.-S. Lee, H. Kim, J.G. Son, Significantly reduced thermal conductivity and enhanced thermoelectric properties of single- and bi-layer graphene nanomeshes with sub-10nm neck-width, Nano Energy 35 (2017) 26–35.
[29] M.C. Nguyen, V.H. Nguyen, H.-V. Nguyen, J. Saint-Martin, P. Dollfus, Enhanced seebeck effect in graphene devices by strain and doping engineering, Physica E 73 (2015) 207–212.
[30] J.A. Lawlor, P.D. Gorman, S.R. Power, C.G. Bezerra, M.S. Ferreira, Sublattice imbalance of substitutionally doped nitrogen in graphene, Carbon 77 (2014) 645–650.
[31] D.Y. Usachov, A.V. Fedorov, O.Y. Vilkov, A.E. Petukhov, A.G. Rybkin, A. Ernst, M.M. Otrokov, E.V. Chulkov, I.I. Ogorodnikov, M.V. Kuznetsov, et al., Large-scale sublattice asymmetry in pure and boron-doped graphene, Nano Lett. 16 (7) (2016) 4535–4543.
[32] L. Caputo, V.H. Nguyen, J.C. Charlier, First-principles study of the structural and electronic properties of BN-ring doped graphene, Phys. Rev. Mater. 6 (11) (2022) 114001.
[33] H. Sawahata, M. Maruyama, N.T. Cuong, H. Omachi, H. Shinohara, S. Okada, Band-gap engineering of graphene heterostructures by substitutional doping with B_3N_3, ChemPhysChem 19 (2) (2018) 237–242.
[34] C. Sánchez-Sánchez, S. Brüller, H. Sachdev, K. Müllen, M. Krieg, H.F. Bettinger, A. Nicolaï, V. Meunier, L. Talirz, R. Fasel, et al., On-surface synthesis of BN-substituted heteroaromatic networks, ACS Nano 9 (9) (2015) 9228–9235.
[35] C. Chen, K. Guo, Y. Zhu, F. Wang, W. Zhang, H. Qi, Construction of layered B_3N_3-doped graphene sheets from an acetylenic compound containing B_3N_3 by a semisynthetic strategy, ACS Appl. Mater. Interfaces 11 (36) (2019) 33245–33253.
[36] S. Mann, I. Mudahar, H. Sharma, V. Jindal, G.S. Dubey, G. Gumbs, V. Fessatidis, Lattice thermal conductivity of pure and doped (B, N) graphene, Mater. Res. Expr. 7 (9) (2020) 095003.
[37] N.R. Abdullah, H.O. Rashid, M.T. Kareem, C.-S. Tang, A. Manolescu, V. Gudmundsson, Effects of bonded and non-bonded B/N codoping of graphene on its stability, interaction energy, electronic structure, and power factor, Phys. Lett. A 384 (12) (2020) 126350.
[38] B. Mortazavi, S. Ahzi, Molecular dynamics study on the thermal conductivity and mechanical properties of boron doped graphene, Solid State Commun. 152 (15) (2012) 1503–1507.
[39] H. Sevinçli, W. Li, N. Mingo, G. Cuniberti, S. Roche, Effects of domains in phonon conduction through hybrid boron nitride and graphene sheets, Phys. Rev. B 84 (20) (2011) 205444.
[40] K. Yang, Y. Chen, R. D'Agosta, Y. Xie, J. Zhong, A. Rubio, Enhanced thermoelectric properties in hybrid graphene/boron nitride nanoribbons, Phys. Rev. B 86 (2012) 045425.
[41] X. Dong, X.-J. Wang, K.-B. Zhang, M.-Q. Long, S.-H. Tan, X.-F. Peng, The electron transport properties and thermoelectric performance in graphene–boron–nitride-nanoribbon-based heterojunctions, Comput. Mater. Sci. 236 (2024) 112858.
[42] T. Ozaki, Variationally optimized atomic orbitals for large-scale electronic structures, Phys. Rev. B 67 (2003) 155108.
[43] T. Ozaki, H. Kino, Numerical atomic basis orbitals from H to Kr, Phys. Rev. B 69 (2004) 195113.
[44] T. Ozaki, H. Kino, Efficient projector expansion for the ab initio LCAO method, Phys. Rev. B 72 (2005) 045121.
[45] J.P. Perdew, K. Burke, M. Ernzerhof, Generalized gradient approximation made simple, Phys. Rev. Lett. 77 (18) (1996) 3865.
[46] I. Morrison, D. Bylander, L. Kleinman, Nonlocal hermitian norm-conserving vanderbilt pseudopotential, Phys. Rev. B 47 (11) (1993) 6728.
[47] V.H. Nguyen, J.-C. Charlier, Recursive green's functions optimized for atomistic modelling of large superlattice-based devices, J. Comput. Electron. 22 (2023) 1–16.
[48] L. Wirtz, A. Rubio, The phonon dispersion of graphite revisited, Solid State Commun. 131 (3) (2004) 141–152.
[49] Y. Xiao, X.H. Yan, J.X. Cao, J.W. Ding, Y.L. Mao, J. Xiang, Specific heat and quantized thermal conductance of single-walled boron nitride nanotubes, Phys. Rev. B 69 (2004) 205415.
[50] X. Du, I. Skachko, A. Barker, E.Y. Andrei, Approaching ballistic transport in suspended graphene, Nat. Nanotechnol. 3 (2008) 491.
[51] K.I. Bolotin, K. Sikes, Z. Jiang, M. Klima, G. Fudenberg, J. Hone, P. Kim, H.L. Stormer, Ultrahigh electron mobility in suspended graphene, Solid State Commun. 146 (9–10) (2008) 351–355.
[52] C.R. Dean, A.F. Young, I. Meric, C. Lee, L. Wang, S. Sorgenfrei, K. Watanabe, T. Taniguchi, P. Kim, K.L. Shepard, et al., Boron nitride substrates for high-quality graphene electronics, Nat. Nanotechnol. 5 (10) (2010) 722–726.
[53] A.S. Mayorov, R.V. Gorbachev, S.V. Morozov, L. Britnell, R. Jalil, L.A. Ponomarenko, P. Blake, K.S. Novoselov, K. Watanabe, T. Taniguchi, et al., Micrometer-scale ballistic transport in encapsulated graphene at room temperature, Nano Lett. 11 (6) (2011) 2396–2399.
[54] E. Munoz, J. Lu, B.I. Yakobson, Ballistic thermal conductance of graphene ribbons, Nano Lett. 10 (5) (2010) 1652–1656.
[55] X. Liu, X. Ma, H. Gao, X. Zhang, H. Ai, W. Li, M. Zhao, Valley-selective circular dichroism and high carrier mobility of graphene-like BC_6N, Nanoscale 10 (27) (2018) 13179–13186.
[56] J. Wang, R. Zhao, Z. Liu, Z. Liu, Widely tunable carrier mobility of boron nitride-embedded graphene, Small 9 (8) (2013) 1373–1378.
[57] Y.M. Zuev, W. Chang, P. Kim, Thermoelectric and magnetothermoelectric transport measurements of graphene, Phys. Rev. Lett. 102 (2009) 096807.
[58] L. Ci, L. Song, C. Jin, D. Jariwala, D. Wu, Y. Li, A. Srivastava, Z. Wang, K. Storr, L. Balicas, et al., Atomic layers of hybridized boron nitride and graphene domains, Nature Mater. 9 (5) (2010) 430–435.
[59] N. Herrera-Reinoza, A.C. dos Santos, L.H. de Lima, R. Landers, A. de Siervo, Atomically precise bottom-up synthesis of h-BNC: graphene doped with h-BN nanoclusters, Chem. Mater. 33 (8) (2021) 2871–2882.
[60] A.A. Balandin, S. Ghosh, W. Bao, I. Calizo, D. Teweldebrhan, F. Miao, C.N. Lau, Superior thermal conductivity of single-layer graphene, Nano Lett. 8 (2008) 902.
[61] V. Hung Nguyen, M.C. Nguyen, H.-V. Nguyen, J. Saint-Martin, P. Dollfus, Enhanced thermoelectric figure of merit in vertical graphene junctions, Appl. Phys. Lett. 105 (13) (2014) 133105.
[62] H. Sadeghi, S. Sangtarash, C.J. Lambert, Cross-plane enhanced thermoelectricity and phonon suppression in graphene/MoS2 van der Waals heterostructures, 2D Mater. 4 (1) (2016) 015012.
[63] D. Olaya, M. Hurtado-Morales, D. Gómez, O.A. Castañeda-Uribe, Z.-Y. Juang, Y. Hernández, Large thermoelectric figure of merit in graphene layered devices at low temperature, 2D Mater. 5 (1) (2017) 011004.
[64] D. Olaya, C.-C. Tseng, W.-H. Chang, W.-P. Hsieh, L.-J. Li, Z.-Y. Juang, Y. Hernández, Cross-plane thermoelectric figure of merit in graphene - C60 heterostructures at room temperature, FlatChem 14 (2019) 100089.